Lithos 231 (2015) 92–102

Contents lists available at ScienceDirect

Lithos

journal homepage: www.elsevier.com/locate/lithos

Zircon U–Pb ages and geochemical characteristics of granitoids in Nagqu area, Tibet

Sai-Jun Sun [a,b], Wei-Dong Sun [a,c,*], Li-Peng Zhang [a,b], Rong-Qing Zhang [a], Cong-Ying Li [a], Hong Zhang [d], Yong-Bin Hu [a,b], Zhao-Rong Zhang [e]

[a] CAS Key Laboratory of Mineralogy and Metallogeny, Guangzhou Institute of Geochemistry, Chinese Academy of Sciences, Guangzhou 510640, China
[b] University of Chinese Academy of Sciences, Beijing 100049, China
[c] CAS Center for Excellence in Tibetan Plateau Earth Sciences, Chinese Academy of Science, Beijing 100101, China
[d] State Key Laboratory of Continental Dynamics, Department of Geology, Northwest University, Xi'an 710069, China
[e] The Western Geological Party of Fujian, Xiamen 361004, China

A R T I C L E I N F O

Article history:
Received 14 November 2014
Accepted 7 June 2015
Available online 15 June 2015

Keywords:
Northern Lhasa subterrane
Early Cretaceous
Granitoids
Zircon Hf–O isotopes
Slab window opening
Crustal growth

A B S T R A C T

This paper reports zircon LA-ICP-MS U–Pb ages and Hf–O isotopic ratios, and whole-rock major and trace element data of Early Cretaceous felsic intrusive rocks from Nagqu area, the northern Lhasa subterrane, southern Tibet. LA-ICP-MS zircon U–Pb dating of biotite granites and biotite monzogranites in the area yields magmatic crystallization ages of ca. 112 Ma, which suggests that they were emplaced in the late Early Cretaceous. Both rocks show high-K calc-alkaline to shoshonitic composition and slightly–moderately peraluminous signature. They are enriched in the alkalis, Rb, Th, K, U and light rare earth elements, depleted in Nb, Ta, Ti and P, and characterized by high Al_2O_3 contents (12–16 wt.%), high Rb/Sr ratios (1.3–33) and low $Mg^{\#}$ values (15–39). Their magmatic zircons have negative $\varepsilon_{Hf}(t)$ values (from −25.9 to 0.5) and high positive $\delta^{18}O$ values (from 7.9‰ to 11.5‰). All the above characteristics indicate that Nagqu biotite monzogranites and biotite granites were likely derived from hybrid melts of sediments from the continent crust with minor mantle-derived input, then experienced varied degrees of fractional crystallization. The Nagqu intrusion is a component of the late Early Cretaceous magmatic flare-up event that occurred during ~120–100 Ma in the northern and partly central Lhasa subterranes. This magmatic flare-up is marked with a great compositional diversity (basalt, rhyolite, adakitic rocks, dioritic enclave, biotite monzogranite and granite) that might be caused by the slab breakoff of the southward subducting Bangong–Nujiang oceanic lithosphere, or more likely by slab window opening, which may have significantly contributed to juvenile crustal growth of the northern Lhasa subterrane.

1. Introduction

Lhasa Terrane generally refers to the EW narrow area between the Bangong–Nujiang suture zone (BNSZ) in the north and Indus–Yarlung Zangbo suture zone (IYZSZ) in the south, with a length of ~2500 km, a width of 150–300 km, which covers an area of ~4.5×10^5 km^2. It includes Precambrian crystalline basement and Paleozoic to Mesozoic sedimentary cover (Zhang et al., 2014). It also experienced the Cenozoic India–Asia continental collision and Jurassic–Cretaceous Lhasa–Qiangtang continental collision (Yin and Harrison, 2000; Zhu et al., 2013). Magmatic rocks of Mesozoic to Miocene ages are widely spread in the Lhasa Terrane (Chen et al., 2011; Hu et al., 2015; Zheng et al., 2012; Zhu et al., 2008a,b, 2009a,d, 2011). Previous studies mainly focused on the central and southern Lhasa subterranes. The magmatic origin and the petrogenesis of magmatic rocks in the central and northern Lhasa subterranes were not well constrained.

Many Early Cretaceous magmatism in the northern and central Lhasa subterranes has been reported (Zhu et al., 2009d). However, the interpretations of the magmatic petrogenesis and geodynamic setting of the northern Lhasa subterrane during the Early Cretaceous are still in dispute. Some works argued that the magmatism was associated with the northward subduction of Neo-Tethyan oceanic crust (Coulon et al., 1986; Ding et al., 2003; Pearce and Mei, 1988). Others suggested that it was related to the thickened crustal anatexis after collision (Harris et al., 1988a,b, 1990; Pearce and Houjun 1988; Xu et al., 1985). Recent studies suggested that the magmatism of the central and northern Lhasa subterranes was correlated to the northward subduction of the Neo-Tethyan oceanic crust in the Early Cretaceous and the southward subduction of the Bangong–Nujiang oceanic crust and subsequent slab break-off (Chen et al., 2010; Huang et al., 2012; Pan et al., 2006; Zhang et al., 2010a,b, 2011; Zhu et al., 2008c, 2009d, 2011, 2013). Although the slab break-off model can plausibly explain the compositional diversity and different tectonic settings, direct petrological and

* Corresponding author at: CAS Key Laboratory of Mineralogy and Metallogeny, Guangzhou Institute of Geochemistry, Chinese Academy of Sciences, Guangzhou 510640, China.
E-mail address: weidongsun@gig.ac.cn (W.-D. Sun).

http://dx.doi.org/10.1016/j.lithos.2015.06.003
0024-4937/

geochemical evidences are still deficient. In this paper, we report in-situ zircon U–Pb dating and Hf–O isotopic compositions, whole-rock major and trace element compositions of granites from the Nagqu area. Our work, together with recently published data, reveals diverse tectono-magmatic processes. Such complex processes offer perspectives on the magmatic origin and the evolution of the crustal growth in the Lhasa Terrane.

2. Geological background and sample description

The study area is located in the hinterland of Qinghai–Tibet plateau, the northern part of the Tibet Autonomous Region (Fig. 1), E92°15′00″–92°45′00″ in longitude and N31°00′00″–31°20′00″ in latitude, closed to the Nagqu County. Tectonically, it is the suture zone of two plates. The southern part is the northern edge of the Gandise–Nyainqentanglha plate (Sangxiong–Maidika continental margin arc magmatic belt is part of the Gandise–Nyainqentanglha plate). The northern part is the Bangong–Nujiang suture zone (Institute of Geological Survey of Tibet Autonomous Region, 2002). It is located in the Sangxiong–Maidika stratigraphic zone, which belongs to Bangor–Basu stratigraphic area. The outcropping strata is mainly composed of Mesozoic and Cenozoic strata, including the Middle Jurassic Mali Formation (J_2m), the Sangkalayong Formation (J_2s), the Early to Middle Jurassic Lagongtang Formation ($J_{2-3}l$), the Cretaceous Duoni Formation (K_1d), the Paleocene–Eocene Niubao Formation ($E_{1-2}n$) and the Quaternary (Fujian Institute of Geological Survey, 2012). Mesozoic volcanic rocks, which are less popular in this region, are mainly in the north of the Gongtusongke area. They belong to intermediate volcanic rocks of the Middle Jurassic Lagongtang Formation. The late Early Cretaceous intrusive rocks are green to white, with thick strip texture and distribute in the Songchagongma belt.

Late Early Cretaceous intermediate and felsic intrusive rocks are well developed in the region, covering a quarter of the whole area. These intrusive rocks are composed of medium- to coarse-grained

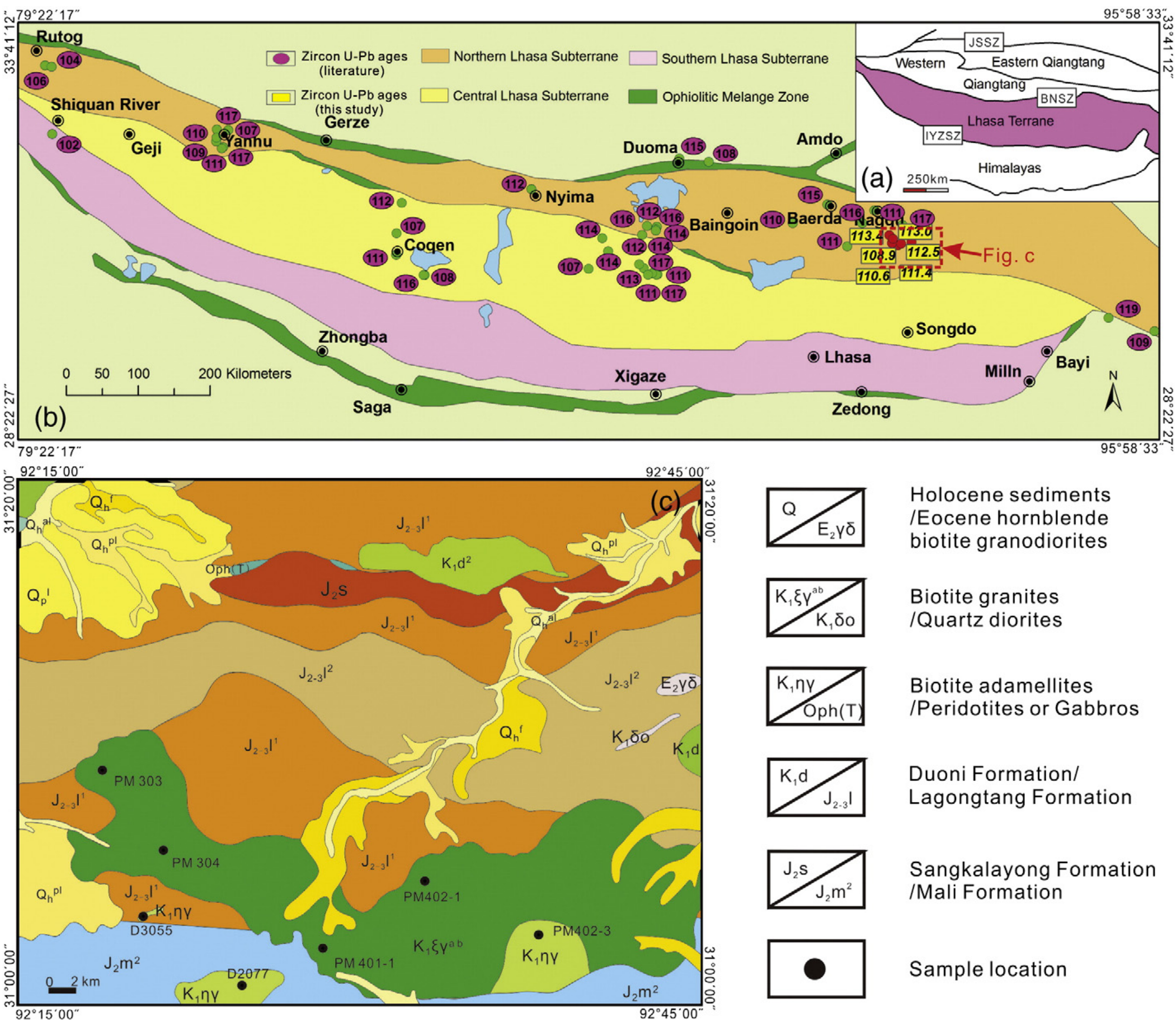

Fig. 1. (a) Tectonic subdivision of the Tibetan Plateau (Zhu et al., 2011). (b) The tectonic framework of the Lhasa Terrane and the localities of magmatic rocks dated at ca. 112 Ma (modified by Sui et al., 2013). (c) Geological map of the studied area. Abbreviations: JSSZ = Jinsha Suture Zone; BNSZ = Bangong–Nujiang Suture Zone; IYZSZ = Indus–Yarlung Zangbo Suture Zone. Literature data are compiled from Chen et al. (2014), Ma (2013), Chiu et al. (2009), Sui et al. (2013), Yu, 2010 and Zhu et al. (2009b, 2011).

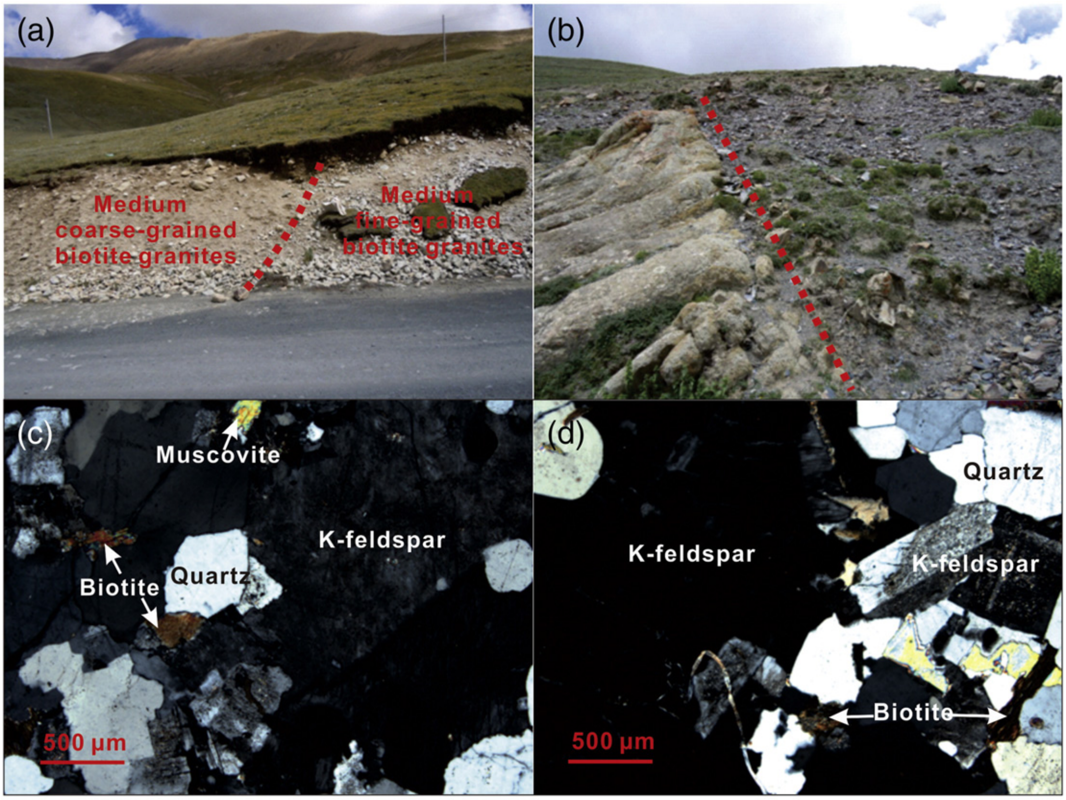

Fig. 2. (a–b) Field contacts of biotite granites and biotite monzogranites from Nagqu area in the northern Lhasa subterrane. (c–d) Photomicrographs of biotite granites and biotite monzogranites from the Nagqu area (cross-polarized light).

biotite granites ($K_1\xi\gamma$) and medium-grained biotite monzogranites ($K_1\eta\gamma$).

1). Early Cretaceous medium-grained biotite granites ($K_1\xi\gamma$): These granites expose in the Lanamula belt of the north Sangdigongshe of the Nagqu county, forming the Maidika batholith (irregular strip, E–W spreading, an area of about 150 km^2). From the central phase to the marginal phase, the batholith consists of medium-grained biotite granites and medium- to coarse-grained biotite granites, with gradual transition in between (Fig. 2a). The samples have massive structure and medium-grained granitic or cataclastic texture, ranging from 2 to 7 mm in mineral particle. The rock-forming minerals include K-feldspar (50–55%), plagioclase (10–15%), quartz (~25%), biotite (~3%) and muscovite (~1%) (Fig. 2c). K-feldspar is the most abundant mineral and shows Carlsbad twins with subhedral tabular crystals. Plagioclase occurs commonly as subhedral columnar crystals. Quartz occurs as subhedral crystals with strong undulatory extinction. Mica includes biotite with subhedral sheets and muscovite. Accessory minerals include apatite, zircon and epidote.
2). Early Cretaceous medium-grained biotite monzogranites ($K_1\eta\gamma$): The pluton is distributed in the Dasaxianggelala and Sangdi belt, with an area of ~37 km^2 (Fig. 2b). The samples are light gray and have massive structure and medium-grained granitic texture with mineral grain sizes from 2 to 5 mm. Rock-forming minerals comprise plagioclase (~30%), K-feldspar (~34%), quartz (~30%), biotite (2–6%), and muscovite (1–2%) (Fig. 2d). Accessory minerals mainly include tourmaline, apatite and zircon. Plagioclase crystals with subhedral commonly have zonal structure with the development bicrystal. K-feldspar is subhedral orthoclase perthite and occasionally displays Carlsbad twins. Quartz is commonly found as xenomorphic granular texture with internal microfracture and undulatory extinction. Biotite displays euhedral to subhedral leaf shape and brown to light brown yellow pleochroism, with chlorite alteration in its edge and cleavage.

3. Analytical methods

Fresh samples were broken to small pieces, then washed and crushed to 200-mesh. The major and trace elements of the samples were analyzed at the Sanming Laboratory, Fujian Bureau of Geology and Mineral Resources, by using atomic absorption spectrophotometry instrument on GGX-9 and thermoelectric ICP 6300 inductively coupled plasma emission spectrometer, respectively. The analytical precision for major elements was better than 1%, and that of the trace elements was better than 5%.

U–Pb dating of zircons was carried out using LA-ICP-MS, whereas in situ zircon Hf isotopic analyses were conducted on equivalent spots where U–Pb dating was performed on a Neptune MC-ICP-MS, both were coupled with RESOlution M-50 laser ablation system at Guangzhou Institute of Geochemistry, Chinese Academy of Science. In-situ zircon oxygen isotope analyses were carried out using the new SHRIMP IIe/MC at the Beijing SHRIMP Center. The detailed analytical conditions and procedures are described in the Appendix A.

4. Results

4.1. Whole-rock geochemistry

Thirteen samples were analyzed for major and trace element compositions of Nagqu granitoids. The major and trace elements data are summarized in Table S1.

The Nagqu granitoids mostly plot in the granodiorite to alkaline-granite fields of the Q'-ANOR diagram (Fig. 3a), as biotite granites (D2077, D3055, PM304, PM401, PM402-3) and biotite monzogranites

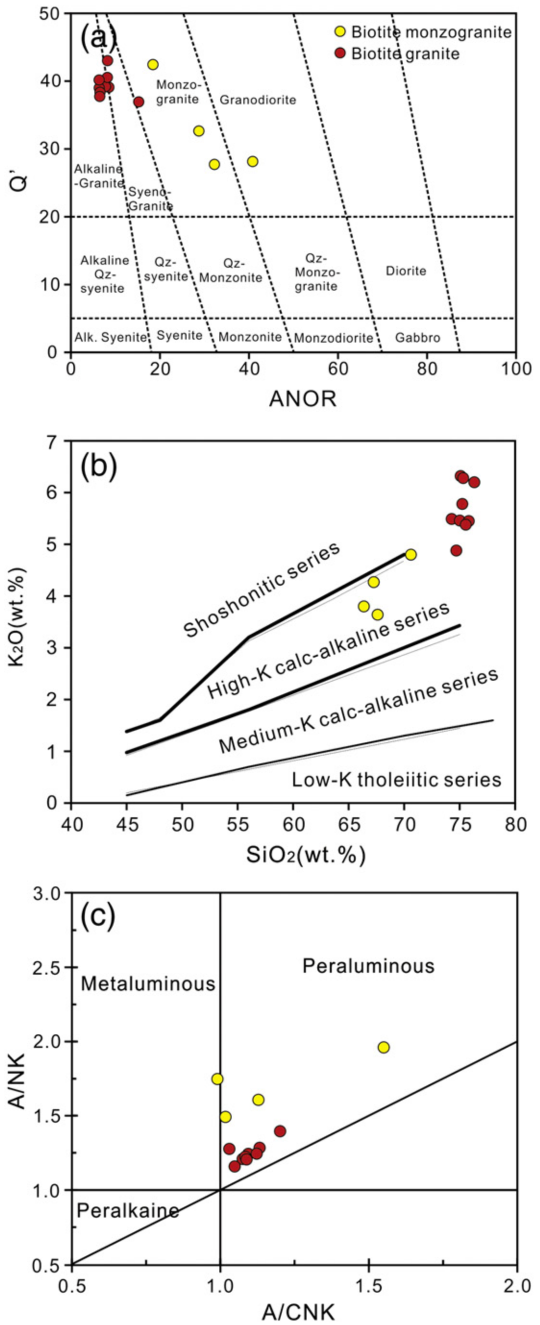

Fig. 3. (a) Q'-ANOR normative composition diagram (Streckeisen and Le Maitre, 1979) for classification of Nagqu granitoids; (b) diagram of SiO_2 versus K_2O; (c) A/NK versus A/CNK diagram for Nagqu granitoids.

(PM303, PM402-1). They show large compositional variations with SiO_2 contents ranging from 66.4 to 76.3 wt.%. The total alkali contents ($Na_2O + K_2O$) vary from 6.0 to 8.6 wt.%. The Mg# values of Nagqu samples range from 15 to 39 (<40). Nagqu biotite monzogranites and biotite granites belong to the high-K calc-alkaline to shoshonitic series (Fig. 3b). In contrast, the Nagqu granitoids are weakly–moderately peraluminous (A/CNK = 0.99–1.55, A/NK = 1.16–1.96) and corundum appeared by calculating CIPW standard minerals (Fig. 3c). The differentiation index of Nagqu granitoids ranges from 71.7 to 94.5. The Nagqu biotite granites have high differentiation index (>90), high SiO_2 (>74–75 wt.%) and high Rb/Sr values, which are similar to previously published Zayu highly fractionated granites (Zhu et al., 2009c). Furthermore, in FeO*/MgO and ($K_2O + Na_2O$)/CaO vs. (Zr + Nb + Ce + Y) diagrams (Fig. 4), Nagqu granitoids fall in the fields ranging from highly fractionated to unfractionated granites. The contents of Al_2O_3, FeO^T, CaO, MgO and TiO_2 systematically decrease (Fig. 5) with increasing SiO_2, suggestive of obvious magmatic differentiation. High differentiation index and FeO^T/MgO ratios (2.78–10.02) also suggest both types of granites experienced significant magmatic differentiation. In addition, the P_2O_5 contents increased or unchanged with increasing SiO_2 contents, and Th contents decreased with increasing Rb contents (Fig. 6). These characteristics are similar to those of S-type granites (Chappell and White, 1992).

In primitive mantle-normalized spider diagrams, Nagqu granitoids show coherent patterns, with high LILEs such as Rb, K, Th and U and low HFSEs such as Nb, Ta, Zr, Hf (Table S1) (Fig. 7a). The total REE contents of Nagqu granitoids range from 60 to 235 ppm. In a chondrite-normalized REE diagram, the samples are characterized by relative enrichments of LREE relative to HREE ($(La/Yb)_N = 3.2$–55.0), with negative Eu anomalies (average $\delta_{Eu} = 0.36$) (Fig. 7b), which indicates removal of plagioclase by fractional crystallization during magma evolution or residual plagioclase during partial melting. Consistently, the negative anomalies of Ba, Sr, Eu also suggest the involvement of plagioclase.

4.2. LA-ICP-MS U–Pb zircon dating

Zircon U–Pb isotope data determined by LA-ICP-MS are listed in Table S2. As CL images indicated, zircon grains have typical oscillatory magmatic zoning with prismatic, colorless, euhedral crystals containing minor inclusions (Fig. S1). Overgrowths of zircon have varied U (88–2591 ppm) and Th (46–1503 ppm) contents with most of the Th/U values ranging from 0.2 to 1.4 (>0.1), indicating magmatic origins (Hoskin and Black, 2000; Sun et al., 2002; Wu and Zheng, 2004). The weighted mean $^{206}Pb/^{238}U$ ages for D2077, D3055, PM303, PM304, PM401-1 and PM402-3 are 111.4 ± 1.2 Ma, 110.6 ± 1.3 Ma, 113.4 ± 1.7 Ma, 113.0 ± 1.4 Ma, 108.9 ± 2.6 Ma and 112.5 ± 1.4 Ma, respectively (Fig. 8), i.e., all the Nagqu granitoids were formed at ~112 Ma, belonging to the late Early Cretaceous. Inherited zircons show $^{206}Pb/^{238}U$ ages of 130–300 Ma. The chondrite-normalized REE patterns of zircon show negative Eu and positive Ce anomalies.

The zircon saturation temperatures (T_{Zr}) of Nagqu granitoids vary from 730 °C to 850 °C (Table S1), with an average of ~770 °C using the method of Watson and Harrison (1983). Ti-in-zircon thermometer is another useful tool, which records the temperature when zircon crystallized (Ferry and Watson, 2007; Watson et al., 2006). Ti-in-zircon temperatures mostly range from 650 °C to 750 °C (Table S5), with an average of ~720 °C, which are systematically colder than the zircon saturation temperature. In general, zircon crystallizes early in intermediate-acid magma, therefore early magmatic zircon crystallization temperature can be taken as the magma temperature (Ferreira et al., 2003; Wu et al., 2007a). For Nagqu granites, the highest zircon saturation temperature is about 100 °C hotter than the Ti-in-zircon temperature indicating the involvement of hot components, likely from the asthenospheric mantle.

Magmatic zircon usually has positive Ce anomaly, the magnitude of which depends on the oxygen fugacity of the magmas. Because of the identical charge and the similar size in eight-fold coordination, Ce^{4+} (with ionic radii of ~0.101 nm) easily substitutes Zr^{4+} (with ionic radii of ~0.098 nm) of zircon under oxidizing conditions, and thus is compatible in zircon (Zhang et al., 2013). In contrast, Ce^{3+} is incompatible in zircon. Therefore, the Ce^{4+}/Ce^{3+} ratios of zircon can reflect the magmatic oxidation states (Ballard et al., 2002). Calculated zircon Ce^{4+}/Ce^{3+} values are listed in Table S5. Most zircon grains with ages of ~112 Ma have relatively low Ce^{4+}/Ce^{3+} ratios (0.1 to 163), indicating low oxygen fugacity (Table S5). This is consistent with the occurrence of ilmenite in the granitoids, indicating of low oxygen fugacities (Ishihara, 1977; Ishihara et al., 2006).

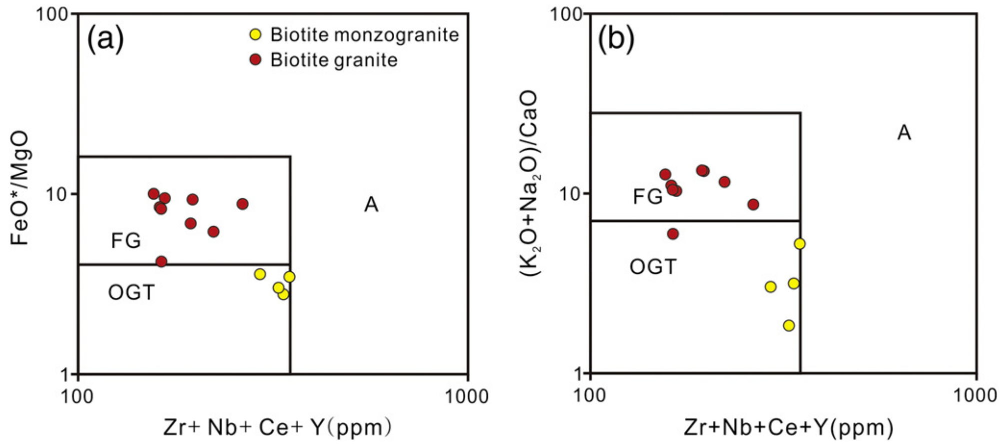

Fig. 4. (a) FeO*/MgO, (b) $(K_2O + Na_2O)/CaO$ vs. (Zr + Nb + Ce + Y) classification diagrams (Whalen et al., 1987). FG: fractionated felsic granites; OGT: unfractionated M-, I- and S-type granites; A: A-type granites; $FeO^* = FeO^T$.

4.3. Zircon Hf isotopes

Five samples were analyzed for Lu–Hf isotopes on the same or similar sites of U–Pb dating. The analytical results are listed in Table S3. Because zircons have extremely low Lu/Hf ratios and their present Hf isotope ratios are similar to those when they crystallized, zircon Hf isotopes are popularly used in geochemical studies (Wu et al., 2007b). For our data, most of $^{176}Lu/^{177}Hf$ ratios are less than 0.002 (ranging from 0.000563 to 0.003843 with an average of ~0.001517), indicating negligible amount of radiogenic ^{177}Hf. Except PM401-1-11 (with a value of 0.281993), $^{176}Hf/^{177}Hf$ values vary from 0.282365 to 0.282700. The corresponding $\varepsilon_{Hf}(t)$ values are from −12.6 to −0.5 (Fig. 9a) and the two-stage Hf model ages (T^C_{DM}) range between 972–1587 Ma, clustering at ~1230 Ma. PM401-1-11 has more negative $\varepsilon_{Hf}(t)$ value (−25.9) and correspondingly older Hf model age (2248 Ma).

4.4. Zircon oxygen isotopes

Zircons are resistant to high-temperature alteration and may retain the original O isotopic compositions due to the low O diffusion coefficient (Wan et al., 2013). Based on the CL images and U–Pb data, only the most unambiguous sites were selected for analysis. The O isotopic compositions of zircons from D3055, PM304, PM401-1 and PM402-3 are listed in Table S4. In-situ zircon O isotope analyses vary from 8‰

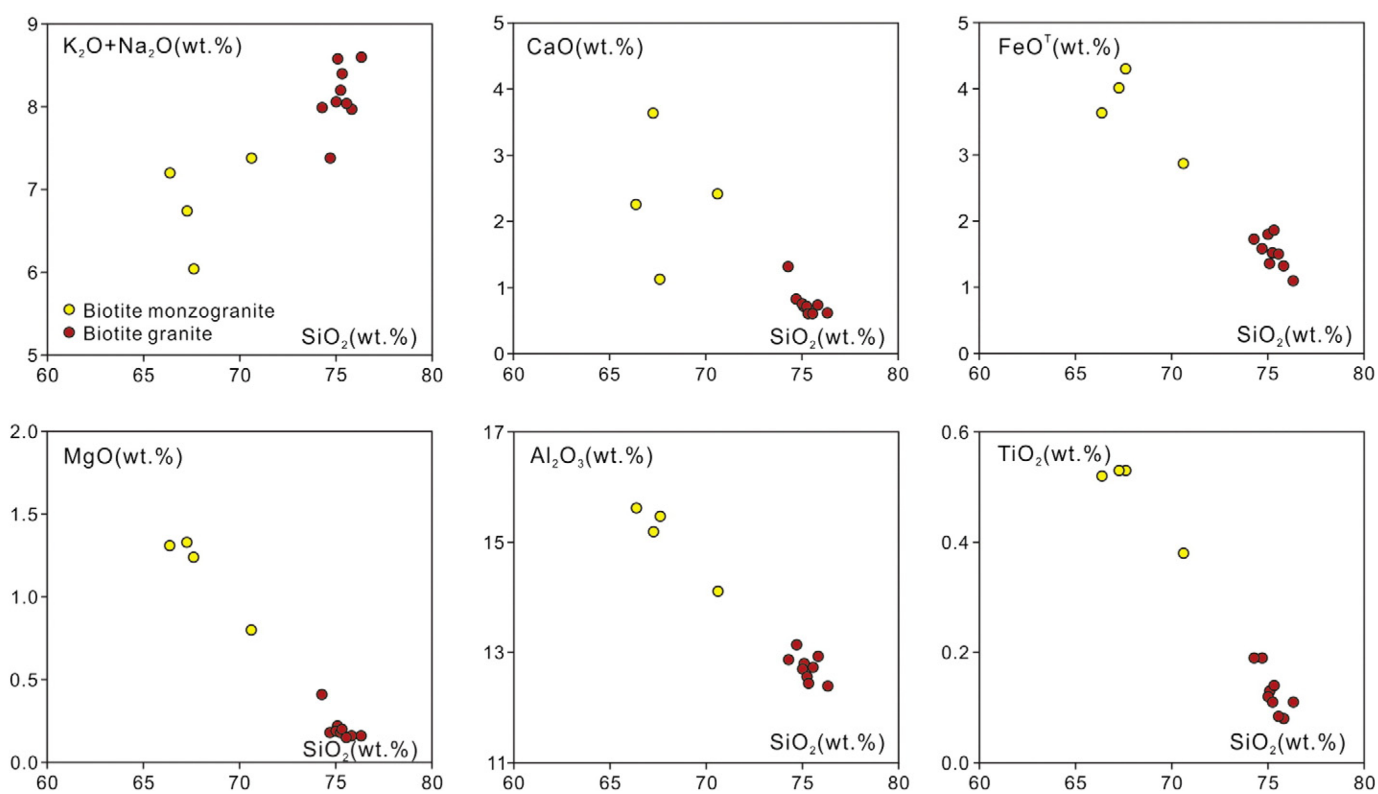

Fig. 5. Harker diagrams for the Nagqu granitoids.

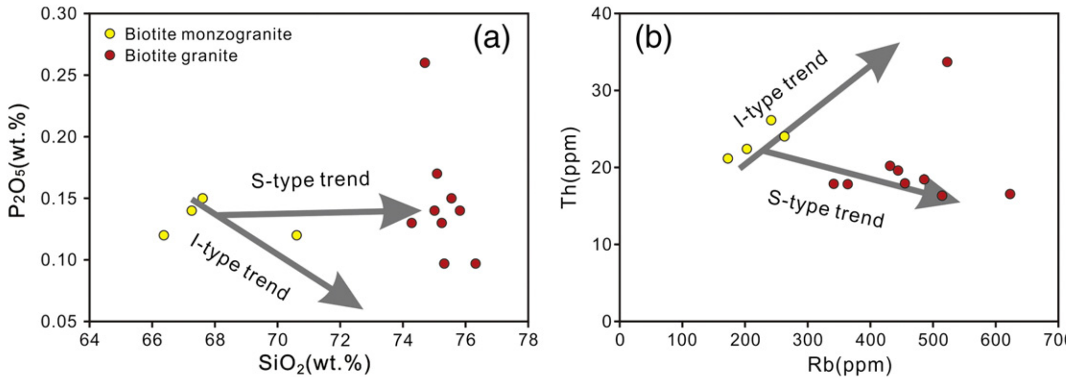

Fig. 6. (a) and (b): P_2O_5 vs. SiO_2 and Th vs. Rb diagrams for identifying I-S type granites (Chappell and White, 1992).

to 11‰ (Fig. 9b) and are higher than those of zircons crystallized from mantle magmas ($\delta^{18}O = 5.3 \pm 0.3‰$) (Valley, 2003; Valley et al., 2005). Melts derived from sedimentary rocks have high $\delta^{18}O$ values, whereas melts from the rocks that suffered high-temperature hydrothermal alteration, have $\delta^{18}O$ values lower than the mantle value (Eiler, 2001; Taylor Jr, 1968; Valley, 2003; Valley et al., 2005). The $\delta^{18}O$ values of the Nagqu granitoids are similar to those of the sediments and may be closely related to the sedimentary rocks in origin.

5. Discussion

5.1. Geochronology

Zircons from biotite monzogranites and biotite granites in the Nagqu region showed similar U–Pb ages (108.9 to 113.4 Ma). Interestingly, this is similar to previous results in other parts of the central and northern of Lhasa subterranes (Fig. 1b) (Chen et al., 2014; Chiu et al., 2009; Ma, 2013; Sui et al., 2013; Yu, 2010; Zhu et al., 2009b, 2011). Magmatic rocks of the late Early Cretaceous are widespread and have diverse compositions in the central and northern Lhasa subterranes, such as mafic enclaves from Xainza and Coqen, granitoids from Samba, dacites from Nyima, mafic enclaves and host granitoids from Rutog, and andesites, rhyolites and granites from Nagqu and Daguo (Chen et al., 2014; Sui et al., 2013; Sun et al., 2015; Zhu et al., 2011). These diverse rock types were synchronously emplaced at ca. 112 Ma (Chen et al., 2014; Sui et al., 2013). The available geochronological data indicates a flare-up of magmatism at ca. 112 Ma in the central and northern Lhasa subterranes, suggesting a major tectonic event along the belt. Nagqu granitoids reported here are likely to be the products of this tectonic event.

5.2. Petrogenesis of Nagqu granitoids

The low-Si unfractionated granites have higher CaO, FeO^T, Al_2O_3, MgO and TiO_2 than the high-Si highly fractionated granites. With increasing SiO_2, both types of granites show similar negative linear trends. Both rocks are enriched in LILEs (Rb, Ba, Th, U, K etc.) and depleted in HFSEs (Nb, Ta, Ti etc.), showing distribution patterns similar to island arc volcanic rocks (Fig. 7). However, comparing to slightly fractionated granites, highly fractionated granites have more negative Ba, Eu, Sr, P, Ti anomalies due to further fractional crystallization. These suggest that both residual and accumulative plagioclase might be responsible to these anomalies.

The high Rb/Sr and low Nb/U indicate materials from the continental crust have important contributions in the generation of these granitoids. The low Ti and P, high Al contents are characteristics of S-type granites. Experimental results indicate that the solubility of apatite increases with increasing SiO_2 contents during magmatic differentiation in peraluminous melts (S-type) (Wolf and London, 1994), while there is an inverse trend in metaluminous to slightly peraluminous melts (I-type) (Zhu et al., 2009c). The Nagqu samples range from slightly to moderately peraluminous, P_2O_5 contents increased or unchanged with increasing SiO_2 contents, and Th contents decreased with increasing Rb contents (Fig. 6). These characteristics are also similar to those of S-type granites (Chappell and White, 1992). However, the absence of

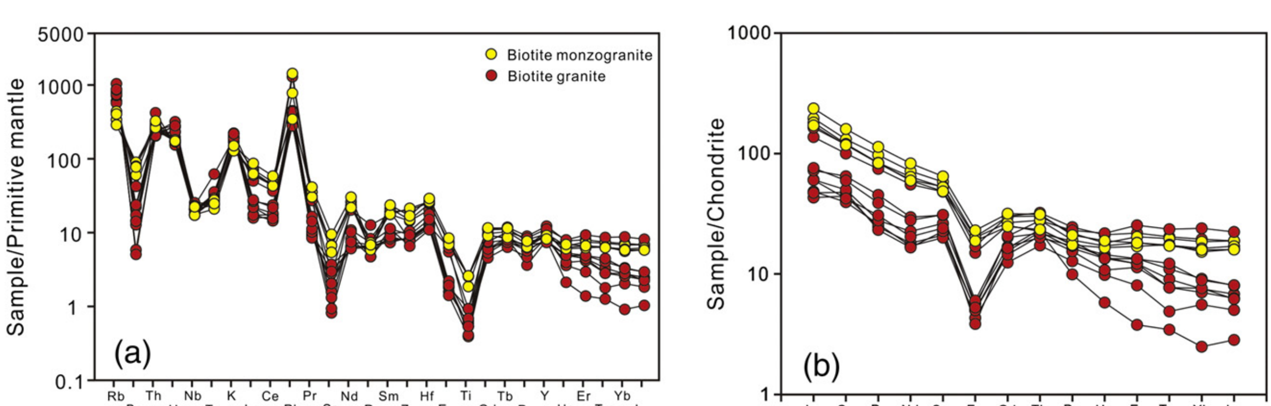

Fig. 7. (a) Primitive mantle-normalized trace elements spider diagrams of Nagqu granitoids; (b) chondrite-normalized REE patterns of Nagqu granitoids. Normalizing values are from Sun and McDonough (1989).

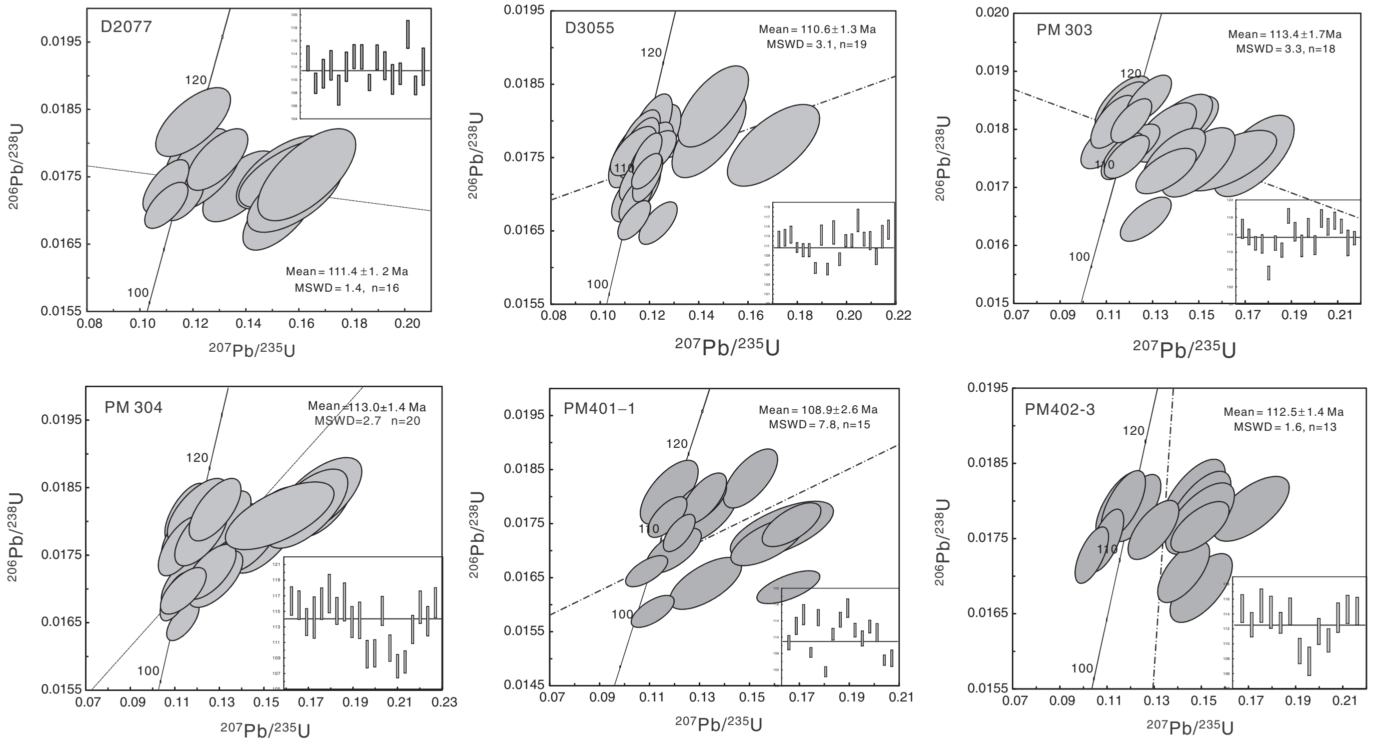

Fig. 8. Zircon U–Pb concordia diagrams of granitoids from the Nagqu area.

typical minerals (muscovite, garnet and cordierite) under microscope indicates that both types of granitoids are most likely to be slightly–moderately peraluminous granites with S-type affinities, which experienced different degrees of fractional crystallization.

Hafnium model ages represent the time when the source rocks were derived from the mantle. In most cases, Hf isotopes of sediments are a mixture of different source rocks. Oxygen isotopes can be used to identify contribution from the supracrustal rocks (those with $\delta^{18}O > 6.5‰$) (Hawkesworth et al., 2010; Kemp et al., 2006). All of our Cretaceous zircon samples have a dispersive range of $\varepsilon_{Hf}(t)$ values (−12.6 to −0.5) and Hf model ages (972–1587 Ma). Such variations in magmatic zircon from a single sample need an open system process to shift the $^{176}Hf/^{177}Hf$ ratio of the melt. The heterogeneous $\varepsilon_{Hf}(t)$ values may come from the mixing between continental crust-derived and mantle-derived components (Kemp et al., 2007). The zircon (102 Ma) with the lowest $\varepsilon_{Hf}(t)$ value (−25.9) has an older Hf model age (2248 Ma), which indicate older mature crustal materials in the Nagqu region. Consistently, Sun et al. (2015) also reported another zircon grain (107.6 Ma) with $\varepsilon_{Hf}(t)$ value (−30.4) in Nagqu volcanic rocks. The granites have $\delta^{18}O$ values higher than mantle-derived magmas (±5.3‰) and are similar to the sedimentary rocks, which are likely derived from an ancient mature crustal source. The covariant ε_{Hf} versus $\delta^{18}O$ diagram (Fig. 10) shows that the mantle contributes no more than 20% to the Nagqu granites. At the same time, both types of granites have high zircon saturation temperatures (730 °C–850 °C), which are similar to Fogang granites with input of mantle-derived components in South China (Li et al., 2007). Most of the unfractionated granites have higher zirconium saturation temperatures (>800 °C), suggestive of input of mantle-derived components (Table S1). As discussed above, Nagqu granitoids are most likely generated by partial melting

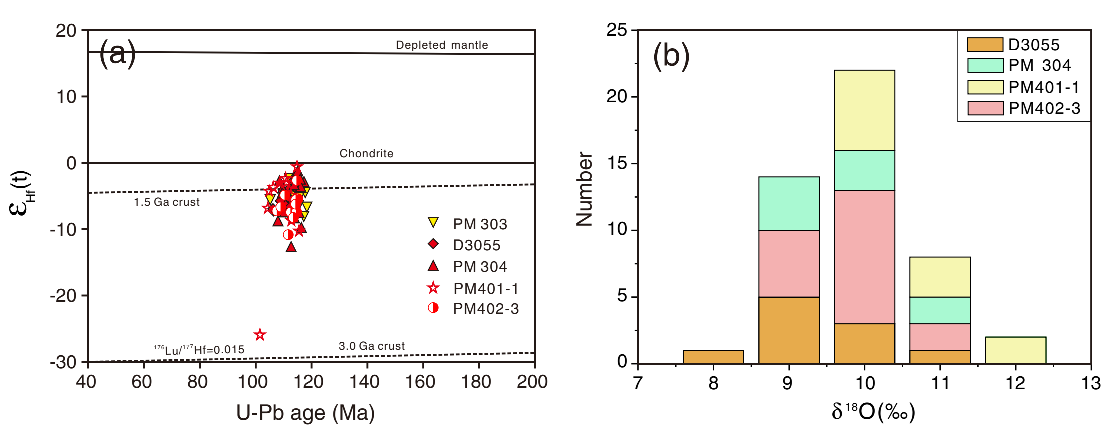

Fig. 9. (a) Relationship between $\varepsilon_{Hf}(t)$ values and U–Pb ages for zircons from Nagqu granitoids (yellow denotes biotite monzogranite; red denotes biotite granite); (b) histogram showing zircon $\delta^{18}O$ values of Nagqu biotite granites.

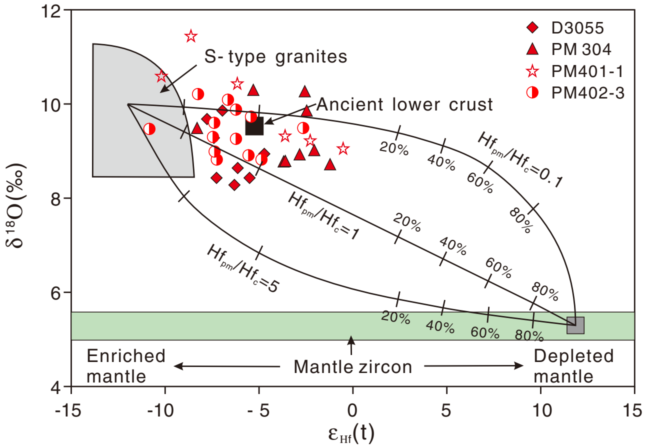

Fig. 10. Plot of $\varepsilon_{Hf}(t)$ versus $\delta^{18}O$ values of zircons from Nagqu biotite granites. The lines denote two-component mixing trends between the mantle- and supercrust-derived magmas. Hf_{pm}/Hf_c is the ratio of Hf concentration in the parental mantle magma (pm) over crustal (c) melt indicated for each curves, and the short lines on the curves represent 20% mixing increments by assuming the mantle zircon has $\varepsilon_{Hf} = 12$ and $\delta^{18}O = 5.3$‰; the crustal zircon has $\varepsilon_{Hf} = -12$ and $\delta^{18}O = 10$‰ (Li et al., 2009); and the lower crust zircon has $\varepsilon_{Hf} = -5.2$ and $\delta^{18}O = 9.4$‰ (Zheng et al., 2012).

of the ancient continental crust mixed with minor mantle-derived melt and have experienced varied degrees of fractional crystallization.

5.3. Tectonic setting and geodynamic interpretation

Geochronological data show a major magmatic flare-up at ~112 Ma in the central and northern Lhasa subterranes (Fig. 1b). The high zircon saturation temperatures of Nagqu granitoids and dispersive and relatively high $\varepsilon_{Hf}(t)$ values indicate input of mantle components. Contemporaneous volcanic rocks in the Nagqu area also provide the evidence of minor input of mantle-derived melt (Huang et al., 2012; Sun et al., 2015). The presence of adakitic rocks, a bimodal volcanic suite and high-Mg basalts indicates different tectonic settings (Chen et al., 2014; Ma, 2013; Chiu et al., 2009; Sui et al., 2013; Yu, 2010; Zhu et al., 2009b, 2011). The contemporaneous magmatic rocks with compositional diversity in the northern Lhasa subterrane was explained by the slab break-off of the southward subducting Bangong–Nujiang Ocean lithosphere (Chen et al., 2014; Sui et al., 2013; Zhu et al., 2009b, 2011).

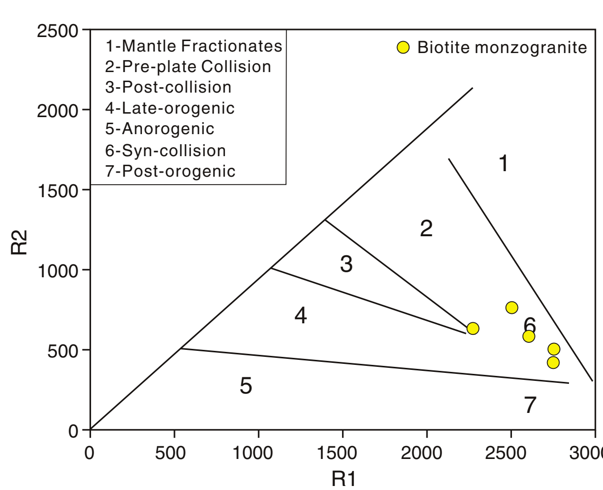

Fig. 11. R1 versus R2 discrimination diagram of Nagqu granitoids. R1 = 4Si-11 (Na + K) − 2(Fe + Ti);R2 = 6Ca + 2 Mg + Al.
After Pearce et al., 1984.

Granites mostly occur in the subduction zones and collision or post-collision extensional settings (Sylvester, 1998; Wu et al., 2007a). On tectonic discrimination diagram, our samples plot in syn-collision and/or post-collision regions (Fig. 11). The presence of post-collision A_2-type granites and rhyolites have been identified in north of Xainza and Daguo, respectively (Chen et al., 2014; Qu et al., 2012), both of which might be related to slab break-off after collision (Ton and Wortel, 1997) or other mantle disturbances.

As mentioned above, the high temperature and short formation time indicate that the most likely heat source for the Nagqu granites is the asthenospheric mantle. In general, slab rollback, slab breakoff, or slab window opening during parallel ridge subduction may all be able to disturb the mantle asthenospheric mantle. Slab rollback, however, usually forms a progressively young magmatic trend, without a distinctive major pulse. Slab window opening opening is equally possible as slab breakoff. Nevertheless, Slab window opening is usually accompanied by adakites and A-type granites.

The slab break-off model cannot feasibly explain the contemporaneous adakites. Sui et al (2013) reported Yanhu quartz dioritic porphyries and dioritic enclaves with adakitic characteristics, which yielded ages of 109.7 ± 0.7 Ma and 110.4 ± 1.4 Ma, respectively. They are contemporaneous with the ca. 112 Ma magmatism in the northern Lhasa subterrane. Therefore, slab window opening is the preferred geodynamic mechanism.

5.4. Implications for crustal growth

It is now well accepted that the continental crust experienced episodic growth. Condie (2013) proposed that most rocks preserved date to the pre-collisional, subduction (ocean-basin closing) stage and not to the collisional stage in Proterozoic orogens. Nevertheless, continental collision on regional scales and super-continental formation on a global scale are episodic, comparing with the continuous process of plate tectonics in terms of seafloor spreading and subduction. Therefore, the episodic growth of the continental crust was explained by continental collision with juvenile crust formation or preservation and super-continent amalgamation (Niu et al., 2013). It is further argued that in the Phanerozoic period, the standard "island arc" model contributes no net mass to the continental crust, for the mass-balanced by subduction erosion and sediment recycling (Niu et al., 2013).

Also, Nagqu granitoids display large range zircon $\varepsilon_{Hf}(t)$ values, Hf model ages and $\delta^{18}O$ values, indicating the magmas derived from mature continental crustal components with mantle-derived melt input. In the tectonic discrimination diagram, the Nagqu samples plot in the syn-collision and post-collision regions (Fig. 11), belonging to the interval between continental subduction and orogen collapse of the complete cycle of continental orogenesis (Song et al., 2014). During exhumation, decompression melting of continental crust is responsible for the generation of granites with S-type granite affinity.

Combined with previous data, there are contemporaneous magmatic rocks with diverse tectonic settings in the northern Lhasa subterrane occurred within ~20 Ma, which can be explained by the slab break-off of the southward subduction (Chen et al., 2014; Sui et al., 2013; Zhu et al., 2009b, 2011). Our recent studies on granitoid rocks and their volcanic analogues formed in response to the Lhasa–Qiangtang continental collision (~112 Ma) show remarkable compositional similarity to the continental crust with typical "arc-like signature" (Sun et al., in 2015). The magmatic flare-up at ~112 Ma in the central and northern Lhasa subterranes indicate input of mantle-derived melt (Sui et al., 2013; Sun et al., 2015; Zhu et al., 2011), which emphasized that processes associated with continental collision produce and preserve the juvenile crust, maintaining the net continental crust growth as previously proposed (Hawkesworth et al., 2010; Niu and O'Hara, 2009; Niu et al., 2013; Sui et al., 2013; Zhu et al., 2011).

6. Conclusion

In-situ zircon U–Pb ages and Hf–O isotopic ratios, whole-rock major and trace element compositions of the late Early Cretaceous magmatic rocks from Nagqu in the northern Lhasa subterrane indicate that:

1) Nagqu granitoids were emplaced at ca. 112 Ma, which are closely related to the Early Cretaceous magmatic flare-up in the northern Lhasa subterrane.
2) Nagqu granitoids exhibit enrichments in LILEs (e.g., Rb, Th, K, U) and LREEs, and depletions in HFSEs (e.g., Nb, Ta, Ti). High Al_2O_3 contents, high Rb/Sr ratios and high $\delta^{18}O$ values indicate major contributions of sedimentary rocks (supra-crustal rocks). They also have highly varied $\varepsilon_{Hf}(t)$ values (from −25.9 to −0.5). All these characteristics indicate that Nagqu granitoids are slightly to moderately peraluminous, and slightly fractionated to highly fractionated granites with the S-type granites affinities. Both types of granites are likely derived from the hybrid melts of old continental components with mantle-derived input, and then experience varied degrees of fractional crystallization.
3) Our study, together with the recent studies revealed that the flare-up of ca. 112 Ma magmatism with diverse geochemical features and tectonic settings either due to slab break-off of the southward subducting Bangong–Nujiang Ocean lithosphere, or more likely triggered by slab window opening, which might had contributed to the crustal growth of the northern Lhasa subterrane.

Supplementary data to this article can be found online at http://dx.doi.org/10.1016/j.lithos.2015.06.003.

Acknowledgments

We thank staff members at the Sanming Laboratory, Fujian Bureau of Geology and Mineral Resources for their assistances in the laboratory, He Li, Chan-Chan Zhang, Hong-Li Zhu, Kai Wu, and Fang Liu for their helpful discussions. The authors would like to thank three anonymous referees for constructive comments, and the editor for constructive suggestions. This work was supported by the National Natural Science Foundation of China (No. 41090374, 41421062 and 91328204). This is contribution No. IS-000 from GIGCAS.

Appendix A

A.1. Analytical methods

Zircon crystals were obtained from Nagqu granitoids using a combination of heavy liquid and magnetic separation techniques, followed by handpicking under a binocular microscope. Zircon grains and TEMORA zircon standard were mounted alongside in epoxy and then polished down to nearly half section. Transmitted and reflected light micrographs as well as cathodoluminescence (CL) images of zircons have been carefully observed to reveal internal structures. U–Pb dating and trace elements analyses were conducted synchronously using LA-ICP-MS at the CAS Key Laboratory of Mineralogy and Metallogeny, Guangzhou Institute of Geochemistry, Chinese Academy of Science. The LA-ICP-MS system is composed of an Agilent 7500 ICP-MS coupled with a Resonetic Resolution M-50 ArF-Excimer laser source ($\lambda = 193$ nm). Instrument operating conditions were 80 mJ laser energy and a repetition rate of 8 Hz with a spot diameter of 33 μm and 40 s ablation time (Li et al., 2012; Liang et al., 2009; Tu et al., 2011). NIST SRM610 glass (Gao et al., 2002; Pearce et al., 1997) and TEMORA zircon standards (Black et al., 2003) were used as external standards. The off-line selection and integration of background and analysis signals, and time-drift correction and quantitative calibration for trace elements and U–Pb dating were performed by ICP-MSDataCal (Liu et al., 2008, 2010). Concordia diagrams and weighted mean calculation were made using Isoplot/Ex_ver3 (Ludwing, 2003). Zircon Ce and Eu anomalies were calculated using software from the Research School of Earth Science, Australian National University (Ballard et al., 2002; Liang et al., 2006).

In situ zircon Hf isotopic analyses were conducted on the equivalent spot where U–Pb dating was performed on a Neptune MC-ICP-MS coupled with RESOlution M-50 laser ablation system at the State Key Laboratory of Isotope Geochemistry, Guangzhou Institute of Geochemistry, Chinese Academy of Science. A spot size of 45 μm with a repetition rate of 8 Hz was applied to the analyses. The Penglai zircon from the Institute of Geology and Geophysics, Chinese Academy of Sciences was used as the reference standard, with a recommended $^{176}Hf/^{177}Hf$ ratio of 0.282906 ± 0.0000010 (2s) (Li et al., 2010). The detailed information was described by Wu et al. (2006).

Oxygen isotope analyses were carried out in Beijing SHRIMP center. The instrument and its operating principles were the same as previously described (Ickert et al., 2008). The SHRIMP IIe/MC was equipped with additional components in order to make high precision O isotopic measurements, including a demountable Cs primary ion source, an electron gun, multicollector and Helmholtz coils. Each $^{18}O/^{16}O$ analysis took about 7 min, the intensity of the Cs^+ primary ion beam was ~3 nA and the spot diameters were ~30 μm in 2008 and ~20 μm in 2010. TEMORA 2 zircon was used as the reference material for calibration of instrumental mass fractionation (IMF) ($\delta^{18}O = 8.20$‰) (Black et al., 2004). At the start of each analytical session, the standard was analyzed, then analyzed after every 3 sample analyses.

References

Ballard, J., Palin, M., Campbell, I., 2002. Relative oxidation states of magmas inferred from Ce(IV)/Ce(III) in zircon: application to porphyry copper deposits of northern Chile. Contributions to Mineralogy and Petrology 144, 347–364.
Black, L.P., Kamo, S.L., Allen, C.M., Aleinikoff, J.N., Davis, D.W., Korsch, R.J., Foudoulis, C., 2003. TEMORA 1: a new zircon standard for Phanerozoic U–Pb geochronology. Chemical Geology 200, 155–170.
Black, L.P., Kamo, S.L., Allen, C.M., Davis, D.W., Aleinikoff, J.N., Valley, J.W., Mundil, R., Campbell, I.H., Korsch, R.J., Williams, I.S., Foudoulis, C., 2004. Improved $^{206}Pb/^{238}U$ microprobe geochronology by the monitoring of a trace-element-related matrix effect; SHRIMP, ID-TIMS, ELA-ICP-MS and oxygen isotope documentation for a series of zircon standards. Chemical Geology 205, 115–140.
Chappell, B., White, A., 1992. I- and S-type granites in the Lachlan Fold Belt. Geological Society of America Special Papers 272, 1–26.
Chen, Y., Zhu, D.C., Zhao, Z.D., Zhang, L.L., Liu, M., Yu, F., Guan, Q., Mo, X.X., 2010. Geochronology, geochemistry and petrogenesis of the Bamco andesites from the northern Gangdese, Tibet. Acta Petrologica Sinica 26, 2193–2206 (in Chinese with English abstract).
Chen, J.L., Xu, J.F., Zhao, W.X., Dong, Y.H., Wang, B.D., Kang, Z.Q., 2011. Geochemical variations in Miocene adakitic rocks from the western and eastern Lhasa terrane: implications for lower crustal flow beneath the southern Tibetan plateau. Lithos 125, 928–939.
Chen, Y., Zhu, D.C., Zhao, Z.D., Meng, F.Y., Wang, Q., Santosh, M., Wang, L.Q., Dong, G.C., Mo, X.X., 2014. Slab breakoff triggered ca. 113 Ma magmatism around Xainza area of the Lhasa Terrane, Tibet. Gondwana Research 26, 449–463.
Chiu, H.Y., Chung, S.L., Wu, F.Y., Liu, D.Y., Liang, Y.H., Lin, I.J., Iizuka, Y., Xie, L.W., Wang, Y.B., Chu, M.F., 2009. Zircon U–Pb and Hf isotopic constraints from eastern Transhimalayan batholiths on the precollisional magmatic and tectonic evolution in southern Tibet. Tectonophysics 477, 3–19.
Condie, K.C., 2013. Preservation and recycling of crust during accretionary and collisional phases of Proterozoic orogens: a bumpy road from Nuna to Rodinia. Geosciences 3, 240–261.
Coulon, C., Maluski, H., Bollinger, C., Wang, S., 1986. Mesozoic and Cenozoic volcanic-rocks from central and southern Tibet — Ar^{39}–Ar^{40} dating, petrological characteristics and geodynamical significance. Earth and Planetary Science Letters 79, 281–302.
Ding, L., Kapp, P., Yin, A., Wang, M., 2003. Early Tertiary volcanism in the Qiangtang terrane of central Tibet: evidence for a transition from oceanic to continental subduction. Journal of Petrology 44, 1833–1865.
Eiler, J.M., 2001. Oxygen isotope variations of basaltic lavas and upper mantle rocks. Stable Isotope Geochemistry 43, 319–364.
Ferreira, V., Valley, J., Sial, A., Spicuzza, M., 2003. Oxygen isotope compositions and magmatic epidote from two contrasting metaluminous granitoids, NE Brazil. Contributions to Mineralogy and Petrology 145, 205–216.
Ferry, J.M., Watson, E.B., 2007. New thermodynamic models and revised calibrations for the Ti-in-zircon and Zr-in-rutile thermometers. Contributions to Mineralogy and Petrology 154, 429–437.
Fujian Institute of Geological Survey., 2012. Regional geological report (1:50000) for Nagqu (in Chinese).
Gao, S., Liu, X.M., Yuan, H.L., Hattendorf, B., Gunther, D., Chen, L., Hu, S.H., 2002. Determination of forty two major and trace elements in USGS and NIST SRM glasses by laser

ablation-inductively coupled plasma-mass spectrometry. Geostandards Newsletter—the Journal of Geostandards and Geoanalysis 26, 181–196.

Harris, N.B.W., Xu, R.H., Lewis, C., Jin, C.W., 1988a. Plutonic rocks of the 1985 Tibet geotraverse, Lhasa to Golmud. Philosophical Transactions of the Royal Society of London. Series A, Mathematical and Physical Sciences 327, 145–168.

Harris, N.B.W., Xu, R.H., Lewis, C.L., Hawkesworth, C.J., Zhang, Y.Q., 1988b. Isotope geochemistry of the 1985 Tibet geotraverse, Lhasa to Golmud. Philosophical Transactions of the Royal Society of London. Series A, Mathematical and Physical Sciences 327, 263–285.

Harris, N.B.W., Inger, S., Xu, R.H., 1990. Cretaceous plutonism in Central Tibet: an example of post-collision magmatism? Journal of Volcanology and Geothermal Research 44, 21–32.

Hawkesworth, C.J., Dhuime, B., Pietranik, A.B., Cawood, P.A., Kemp, A.I.S., Storey, C.D., 2010. The generation and evolution of the continental crust. Journal of the Geological Society 167, 229–248.

Hoskin, P.W.O., Black, L.P., 2000. Metamorphic zircon formation by solid-state recrystallization of protolith igneous zircon. Journal of Metamorphic Geology 18, 423–439.

Hu, Y.B., Liu, J.Q., Ling, M.X., Ding, W., Liu, Y., Zartman, R.E., Ma, X.F., Liu, D.Y., Zhang, C.C., Sun, S.J., Zhang, L.P., Wu, K., Sun, W.D., 2015. The formation of Qulong adakites and their relationship with porphyry copper deposit: geochemical constraints. Lithos 220, 60–80.

Huang, Y., Zhu, D.C., Zhao, Z.D., Zhang, L.L., DePaolo, D., Hu, Z.C., Yuan, H.L., Mo, X.X., 2012. Petrogenesis and implication of the andesites at similar to 113 Ma in the Nagqu region in the northern Lhasa subterrane. Acta Petrologica Sinica 28, 1603–1614 (in Chinese with English abstract).

Ickert, R.B., Hiess, J., Williams, I.S., Holden, P., Ireland, T.R., Lanc, P., Schram, N., Foster, J.J., Clement, S.W., 2008. Determining high precision, in situ, oxygen isotope ratios with a SHRIMP II: analyses of MPI-DING silicate-glass reference materials and zircon from contrasting granites. Chemical Geology 257, 114–128.

Institute of Geological Survey of Tibet Autonomous Region., 2002. Regional geological report (1:250000) for Nagqu (in Chinese).

Ishihara, S., 1977. The magnetite-series and ilmenite-series granitic rocks. Mining Geology 27, 293–305.

Ishihara, S., Ohmoto, H., Anhaeusser, C.R., Imai, A., Robb, L.J., 2006. Discovery of the oldest oxic granitoids in the Kaapvaal Craton and its implications for the redox evolution of early Earth. Geological Society of America Memoirs 198, 67–80.

Kemp, A.I.S., Hawkesworth, C.J., Paterson, B.A., Foster, G.L., Kinny, P.D., Whitehouse, M.J., Maas, R., Eimf, 2006. Exploring the plutonic–volcanic link: a zircon U–Pb, Lu–Hf and O isotope study of paired volcanic and granitic units from southeastern Australia. Transactions of the Royal Society of Edinburgh-Earth Sciences 97, 337–355.

Kemp, A.I.S., Hawkesworth, C.J., Foster, G.L., Paterson, B.A., Woodhead, J.D., Hergt, J.M., Gray, C.M., Whitehouse, M.J., 2007. Magmatic and crustal differentiation history of granitic rocks from Hf–O isotopes in zircon. Science 315, 980–983.

Li, X.H., Li, Z.X., Li, W.X., Liu, Y., Yuan, C., Wei, G., Qi, C., 2007. U–Pb zircon, geochemical and Sr–Nd–Hf isotopic constraints on age and origin of Jurassic I- and A-type granites from central Guangdong, SE China: a major igneous event in response to foundering of a subducted flat-slab? Lithos 96, 186–204.

Li, X.H., Li, W.X., Wang, X.C., Li, Q.L., Liu, Y., Tang, G.Q., 2009. Role of mantle-derived magma in genesis of early Yanshanian granites in the Nanling Range, South China: in situ zircon Hf–O isotopic constraints. Science in China Series D: Earth Sciences 52, 1262–1278.

Li, X.H., Long, W.G., Li, Q.L., Liu, Y., Zheng, Y.F., Yang, Y.H., Chamberlain, K.R., Wan, D.F., Guo, C.H., Wang, X.C., Tao, H., 2010. Penglai zircon megacrysts: a potential new working reference material for microbeam determination of Hf–O isotopes and U–Pb age. Geostandards and Geoanalytical Research 34, 117–134.

Li, H., Ling, M.X., Li, C.Y., Zhang, H., Ding, X., Yang, X.Y., Fan, W.M., Li, Y.L., Sun, W.D., 2012. A-type granite belts of two chemical subgroups in central eastern China: indication of ridge subduction. Lithos 150, 26–36.

Liang, H.Y., Campbell, I.H., Allen, C., Sun, W.D., Liu, C.Q., Yu, H.X., Xie, Y.W., Zhang, Y.Q., 2006. Zircon Ce^{4+}/Ce^{3+} ratios and ages for Yulong ore-bearing porphyries in eastern Tibet. Mineralium Deposita 41, 152–159.

Liang, J.L., Ding, X., Sun, X.M., Zhang, Z.M., Zhang, H., Sun, W.D., 2009. Nb/Ta fractionation observed in eclogites from the Chinese Continental Scientific Drilling Project. Chemical Geology 268, 27–40.

Liu, Y.S., Hu, Z.C., Gao, S., Gunther, D., Xu, J., Gao, C.G., Chen, H.H., 2008. In situ analysis of major and trace elements of anhydrous minerals by LA-ICP-MS without applying an internal standard. Chemical Geology 257, 34–43.

Liu, Y.S., Gao, S., Hu, Z.C., Gao, C.G., Zong, K.Q., Wang, D.B., 2010. Continental and oceanic crust recycling-induced melt–peridotite interactions in the Trans-North China Orogen: U–Pb dating, Hf isotopes and trace elements in zircons from mantle xenoliths. Journal of Petrology 51, 537–571.

Ludwing, K., 2003. User's Manual for ISOPLOT 3.00: A Geochronological Toolkit for Microsoft Excel, Special Publication No. 4. Berkeley Geochronology Center, pp. 1–70.

Ma, Z., 2013. Petrology, geochronology and geochemistry of granitic rocks in Rutog at northern Lhasa terrane, Tibetan plateau (Master Thesis).

Niu, Y.L., O'Hara, M.J., 2009. MORB mantle hosts the missing Eu (Sr, Nb, Ta and Ti) in the continental crust: new perspectives on crustal growth, crust–mantle differentiation and chemical structure of oceanic upper mantle. Lithos 112, 1–17.

Niu, Y.L., Zhao, Z.D., Zhu, D.C., Mo, X.X., 2013. Continental collision zones are primary sites for net continental crust growth—a testable hypothesis. Earth-Science Reviews 127, 96–110.

Pan, G.T., Mo, X.X., Hou, Z.Q., Zhu, D.C., Wang, L.Q., Li, G.M., Zhao, Z.D., Geng, Q.R., Liao, Z.L., 2006. Spatial–temporal framework of the Gangdese Orogenic Belt and its evolution. Acta Petrologica Sinica 22, 521–533 (in Chinese with English abstract).

Pearce, J.A., Mei, H.J., 1988. Volcanic-rocks of the 1985 Tibet geotraverse — Lhasa to Golmud. Philosophical Transactions of the Royal Society a—Mathematical Physical and Engineering Sciences 327, 169–201.

Pearce, J.A., Harris, N.B., Tindle, A.G., 1984. Trace element discrimination diagrams for the tectonic interpretation of granitic rocks. Journal of Petrology 25, 956–983.

Pearce, J.A., Houjun, M., 1988. Volcanic rocks of the 1985 Tibet geotraverse: Lhasa to Golmud. Philosophical Transactions of the Royal Society of London A: Mathematical, Physical and Engineering Sciences 327, 169–201.

Pearce, N.J.G., Perkins, W.T., Westgate, J.A., Gorton, M.P., Jackson, S.E., Neal, C.R., Chenery, S.P., 1997. A compilation of new and published major and trace element data for NIST SRM 610 and NIST SRM 612 glass reference materials. Geostandards Newsletter—the Journal of Geostandards and Geoanalysis 21, 115–144.

Qu, X.M., Wang, R.J., Xin, H.B., Jiang, J.H., Chen, H., 2012. Age and petrogenesis of A-type granites in the middle segment of the Bangonghu–Nujiang suture, Tibetan plateau. Lithos 146, 264–275.

Song, S.G., Niu, Y.L., Su, L., Zhang, C., Zhang, L.F., 2014. Continental orogenesis from ocean subduction, continent collision/subduction, to orogen collapse, and orogen recycling: the example of the North Qaidam UHPM belt, NW China. Earth-Science Reviews 129, 59–84.

Streckeisen, A., Le Maitre, R., 1979. A chemical approximation to the modal QAPF classification of the igneous rocks. Neues Jahrbuch für Mineralogie, Abhandlungen 136, 169–206.

Sui, Q.L., Wang, Q., Zhu, D.C., Zhao, Z.D., Chen, Y., Santosh, M., Hu, Z.C., Yuan, H.L., Mo, X.X., 2013. Compositional diversity of ca. 110 Ma magmatism in the northern Lhasa Terrane, Tibet: implications for the magmatic origin and crustal growth in a continent–continent collision zone. Lithos 168, 144–159.

Sun, S.S., McDonough, W., 1989. Chemical and isotopic systematics of oceanic basalts: implications for mantle composition and processes. Geological Society, London, Special Publications 42, 313–345.

Sun, W.D., Williams, I.S., Li, S.G., 2002. Carboniferous and Triassic eclogites in the western Dabie Mountains, east-central China: evidence for protracted convergence of the North and South China Blocks. Journal of Metamorphic Geology 20 (9), 873–886.

Sun, S.J., Zhang, L.P., Ding, X., Sun, W.D., Zhang, Z.R., 2015. Zircon U–Pb ages, Hf isotopes and geochemical characteristics of volcanic rocks in Nagqu area, Tibet and their petrogenesis. Acta Petrologica Sinica 31 (7), 0000-0000 (in Chinese with English abstract).

Sylvester, P.J., 1998. Post-collisional strongly peraluminous granites. Lithos 45, 29–44.

Taylor Jr., H.P., 1968. The oxygen isotope geochemistry of igneous rocks. Contributions to Mineralogy and Petrology 19, 1–71.

Ton, W.A., Wortel, M., 1997. Slab detachment in continental collision zones: an analysis of controlling parameters. Geophysical Research Letters 24, 2095–2098.

Tu, X.L., Zhang, H., Deng, W.F., Ling, M.X., Liang, H.Y., Liu, Y., Sun, W.D., 2011. Application of RESOlution in-situ laser ablation ICP-MS in trace element analyses. Geochimica 40, 83–98 (in Chinese with English abstract).

Valley, J.W., 2003. Oxygen isotopes in zircon. Zircon 53, 343–385.

Valley, J.W., Lackey, J.S., Cavosie, A.J., Clechenko, C.C., Spicuzza, M.J., Basei, M.A.S., Bindeman, I.N., Ferreira, V.P., Sial, A.N., King, E.M., Peck, W.H., Sinha, A.K., Wei, C.S., 2005. 4.4 billion years of crustal maturation: oxygen isotope ratios of magmatic zircon. Contributions to Mineralogy and Petrology 150, 561–580.

Wan, Y.S., Zhang, J.H., Williams, I.S., Liu, D.Y., Dong, C.Y., Fan, R.L., Shi, Y.R., Ma, M.Z., 2013. Extreme zircon O isotopic compositions from 3.8 to 2.5 Ga magmatic rocks from the Anshan area, North China Craton. Chemical Geology 352, 108–124.

Watson, E.B., Harrison, T.M., 1983. Zircon saturation revisited — temperature and composition effects in a variety of crustal magma types. Earth and Planetary Science Letters 64, 295–304.

Watson, E.B., Wark, D.A., Thomas, J.B., 2006. Crystallization thermometers for zircon and rutile. Contributions to Mineralogy and Petrology 151, 413–433.

Whalen, J.B., Currie, K.L., Chappell, B.W., 1987. A-Type Granites - Geochemical Characteristics, Discrimination and Petrogenesis. Contributions to Mineralogy and Petrology 95, 407–419.

Wolf, M.B., London, D., 1994. Apatite dissolution into peraluminous haplogranitic melts: an experimental study of solubilities and mechanisms. Geochimica Et Cosmochimica Acta 58, 4127–4145.

Wu, Y.B., Zheng, Y.F., 2004. Genesis of zircon and its constraints on interpretation of U–Pb age. Chinese Science Bulletin 49, 1554–1569 (in Chinese with English abstract).

Wu, F.Y., Yang, Y.H., Xie, L.W., Yang, J.H., Xu, P., 2006. Hf isotopic compositions of the standard zircons and baddeleyites used in U–Pb geochronology. Chemical Geology 234, 105–126.

Wu, F.Y., Li, X.H., Yang, J.H., Zheng, Y.F., 2007a. Discussions on the petrogenesis of granites. Acta Petrologica Sinica 23, 1217–1238 (in Chinese with English abstract).

Wu, F.Y., Li, X.H., Zheng, Y.F., Gao, S., 2007b. Lu–Hf isotopic systematics and their applications in petrology. Acta Petrologica Sinica 23 (2), 185–220 (in Chinese with English abstract).

Xu, R.H., Scharer, U., Allegre, C.J., 1985. Magmatism and metamorphism in the Lhasa block (Tibet) — a geochronological study. Journal of Geology 93, 41–57.

Yin, A., Harrison, T.M., 2000. Geologic evolution of the Himalayan–Tibetan orogen. Annual Review of Earth and Planetary Sciences 28, 211–280.

Yu, F., 2010. Petrology, Geochemistry and Petrogenesis of the Granitoid in Southern Yanhu of Gangdese, Tibet (Master Thesis), (in Chinese with English abstract).

Zhang, L.L., Zhu, D.C., Zhao, Z.D., Dong, G.C., Mo, X.X., Guan, Q., Liu, M., Liu, M.H., 2010a. Petrogenesis of magmatism in the Baerda region of Northern Gangdese, Tibet: constraints from geochemistry, geochronology and Sr–Nd–Hf isotopes. Acta Petrologica Sinica 26, 1871–1888 (in Chinese with English abstract).

Zhang, X.Q., Zhu, D.C., Zhao, Z.D., Wang, L.Q., Huang, J.C., Mo, X.X., 2010b. Petrogenesis of the Nixiong pluton in Coqen, Tibet and its potential significance for the Nixiong Fe-rich mineralization. Acta Petrologica Sinica 26, 1793–1804 (in Chinese with English abstract).

Zhang, L.L., Zhu, D.C., Zhao, Z.D., Liao, Z.L., Wang, L.Q., Mo, X.X., 2011. Early Cretaceous granitoids in Xainza, Tibet: evidence of slab break-off. Acta Petrologica Sinica 27, 1938–1948 (in Chinese with English abstract).

Zhang, H., Ling, M.X., Liu, Y.L., Tu, X.L., Wang, F.Y., Li, C.Y., Liang, H.Y., Yang, X.Y., Arndt, N.T., Sun, W.D., 2013. High oxygen fugacity and slab melting linked to Cu mineralization: evidence from Dexing porphyry copper deposits, southeastern China. Journal of Geology 121, 289–305.

Zhang, Z.M., Dong, X., Santosh, M., Zhao, G.C., 2014. Metamorphism and tectonic evolution of the Lhasa terrane, Central Tibet. Gondwana Research 25, 170–189.

Zheng, Y.C., Hou, Z.Q., Li, Q.Y., Sun, Q.Z., Liang, W., Fu, Q., Li, W., Huang, K.X., 2012. Origin of Late Oligocene adakitic intrusives in the southeastern Lhasa terrane: evidence from in situ zircon U–Pb dating, Hf–O isotopes, and whole-rock geochemistry. Lithos 148, 296–311.

Zhu, D.C., Mo, X.X., Zhao, Z.D., Xu, J.F., Zhou, C.Y., Sun, C.G., Wang, L.Q., Chen, H.H., Dong, G.C., Zhou, S., 2008a. Zircon U–Pb geochronology of Zenong Group volcanic rocks in Coqen area of the Gangdese, Tibet and tectonic significance. Acta Petrologica Sinica 24, 401–412 (in Chinese with English abstract).

Zhu, D.C., Pan, G.T., Chung, S.L., Liao, Z.L., Wang, L.Q., Li, G.M., 2008b. SHRIMP zircon age and geochemical constraints on the origin of lower Jurassic volcanic rocks from the Yeba formation, Southern Gangdese, south Tibet. International Geology Review 50, 442–471.

Zhu, D.C., Pan, G.T., Wang, L.Q., Mo, X.X., Zhao, Z.D., Zhou, C.Y., Liao, Z.L., Dong, G.C., Yuan, S.H., 2008c. Tempo-spatial variations of Mesozoic magmatic rocks in the Gangdese belt, Tibet, China, with a discussion of geodynamic setting-related issues. Geological Bulletin of China 27, 1535–1550 (in Chinese with English abstract).

Zhu, D.C., Chung, S.L., Mo, X.X., Zhao, Z.D., Niu, Y.L., Song, B., Yang, Y.H., 2009a. The 132 Ma Comei-Bunbury large igneous province: remnants identified in present-day southeastern Tibet and southwestern Australia. Geology 37, 583–586.

Zhu, D.C., Mo, X.X., Niu, Y.L., Zhao, Z.D., Wang, L.Q., Liu, Y.S., Wu, F.Y., 2009b. Geochemical investigation of Early Cretaceous igneous rocks along an east–west traverse throughout the central Lhasa Terrane, Tibet. Chemical Geology 268, 298–312.

Zhu, D.C., Mo, X.X., Wang, L.Q., Zhao, Z.D., Niu, Y.L., Zhou, C.Y., Yang, Y.H., 2009c. Petrogenesis of highly fractionated I-type granites in the Zayu area of eastern Gangdese, Tibet: constraints from zircon U–Pb geochronology, geochemistry and Sr–Nd–Hf isotopes. Science in China Series D-Earth Sciences 52, 1223–1239.

Zhu, D.C., Zhao, Z.D., Pan, G.T., Lee, H.Y., Kang, Z.Q., Liao, Z.L., Wang, L.Q., Li, G.M., Dong, G.C., Liu, B., 2009d. Early cretaceous subduction-related adakite-like rocks of the Gangdese Belt, southern Tibet: products of slab melting and subsequent melt–peridotite interaction? Journal of Asian Earth Sciences 34, 298–309.

Zhu, D.C., Zhao, Z.D., Niu, Y.L., Mo, X.X., Chung, S.L., Hou, Z.Q., Wang, L.Q., Wu, F.Y., 2011. The Lhasa Terrane: record of a microcontinent and its histories of drift and growth. Earth and Planetary Science Letters 301, 241–255.

Zhu, D.C., Zhao, Z.D., Niu, Y.L., Dilek, Y., Hou, Z.Q., Mo, X.X., 2013. The origin and pre-Cenozoic evolution of the Tibetan Plateau. Gondwana Research 23, 1429–1454.